Journal of
Synchrotron
Radiation

ISSN 0909-0495

Received 11 August 2010
Accepted 23 November 2010

Rietveld and pair distribution function study of Hägg carbide using synchrotron X-ray diffraction

Hester Esna du Plessis,[a] J. P. R. de Villiers,[b] G. J. Kruger,[c] A. Steuwer[d,e]* and M. Brunelli[f]

[a]Sasol Technology R&D, South Africa, [b]University of Pretoria, South Africa, [c]University of Johannesburg, South Africa, [d]ESS AB, Stora Algatan 4, 22100 Lund, Sweden, [e]NMMU, Port Elizabeth 6031, South Africa, and [f]Institut Laue-Langevin, BP 156, 38042 Grenoble Cedex 9, France. E-mail: axel.steuwer@esss.se

Fischer–Tropsch (FT) synthesis is an important process in the manufacturing of hydrocarbons and oxygenated hydrocarbons from mixtures of carbon monoxide and hydrogen (syngas). The reduced iron catalyst reacts with carbon monoxide and hydrogen to form bulk Fe_5C_2 Hägg carbide (χ-HC) during FT synthesis. Arguably, χ-HC is the predominant catalyst phase present in the working iron catalyst. Deactivation of the working catalyst can be due to oxidation of χ-HC to iron oxide, a step-wise decarburization to cementite (θ-Fe_3C), carbon formation or sintering with accompanying loss of catalytic performance. It is therefore critical to determine the precise crystal structure of χ-HC for the understanding of the synthesis process and for comparison with the first-principles *ab initio* modelling. Here the results of high-resolution synchrotron X-ray powder diffraction data are reported. The atomic arrangement of χ-HC was confirmed by Rietveld refinement and subsequent real-space modelling of the pair distribution function (PDF) obtained from direct Fourier transformation. The Rietveld and PDF results of χ-HC correspond well with that of a pseudo-monoclinic phase of space group $P\bar{1}$ [a = 11.5661 (6) Å, b = 4.5709 (1) Å, c = 5.0611 (2) Å, α = 89.990 (5)°, β = 97.753 (4)°, γ = 90.195 (4)°], where the Fe atoms are located in three distorted prismatic trigonal and one octahedral arrangement around the central C atoms. The Fe atoms are distorted from the prismatic trigonal arrangement in the monoclinic structure by the change in C atom location in the structure.

Keywords: Hägg carbide; Fischer–Tropsch synthesis; crystal structure; PDF.

1. Introduction

Recent fluctuating oil prices and increasing environmental concerns have stimulated renewed interest in the production of synthetic hydrocarbons (fuels) by Fischer–Tropsch synthesis (FTS) using biomass, natural gas or coal as starting material (Dry, 1990; Riedel & Schulz, 2003*a*,*b*; Campos *et al.*, 2010). The FTS involves a catalyst, and one of the most commonly used commercial catalyst is Fe-based, starting from oxides with small amounts of promoter substances such as Cu, K, SiO_2 added to improve performance (Herranz *et al.*, 2006; Niemantsverdriet *et al.*, 1980). The Fe catalysts require an activation pre-treatment (using CO, syngas, hydrogen) and, in order to increase the efficiency, nanoscale oxide powders with high surface-to-bulk ratios are being used (Sarkar *et al.*, 2007). During activation the iron oxides evolve, resulting in the formation of metallic iron and a range of carbides depending on temperature, pressure of carbon-containing gases, concentration, time of exposure, *etc.* Subsequent annealing results in a diffusion-determined de-carburization process forming stable cementite. Cementite and other iron carbide phases have also been observed to form *via* lattice-invariant deformation after carbon ion implantation into thin iron layers (Königer *et al.*, 1997). Experimental evidence suggests that the activity (and hence performance) of the Fe-based catalyst is critically dependent on the presence and type of carbides on the surface (Herranz *et al.*, 2006). There is a range of meta-stable and stable iron carbides, and the differences in crystal structure are relatively subtle but distinct, and can be confirmed with the aid of electron diffraction (Hirotsu & Nagakura, 1972; du Plessis *et al.*, 2007). In general, the iron carbides can be divided into carbides with C atoms on octahedral interstitial sites (O-carbides) such as ε-Fe_2C, ε'-$Fe_{2.2}C$ and Fe_xC, and carbides with C atoms on trigonal prismatic interstices such as η-Fe_2C and χ-Fe_5C_2 (Hägg) and the (stable) cementite phase θ-Fe_3C. The exact nature of the carbonaceous

species on the surface and in the bulk over the catalyst has been the subject of intense investigations over recent years (Herranz *et al.*, 2006; Steynberg *et al.*, 2008; Faraoun *et al.*, 2006; Mansker, 1999; Pérez-Alonso *et al.*, 2007), but experimental evidence points at the Hägg carbide being the prevalent phase under 'steady-state' FTS conditions and principally responsible for FTS activity. During FTS the partial pressure of syngas is kept constant, promoters are added to aid the dissociation of carbon and oxygen on the catalyst surface, and the de-carburization process of Hägg carbide to cementite is thus limited.

The oxidation of iron and iron carbides to magnetite is a postulated deactivation mechanism of the catalyst, owing to the water–gas shift reaction taking place (Sarkar *et al.*, 2007; Mansker, 1999). Molecular dynamic simulation studies of the interaction of carbon with self-interstitial clusters in α-iron indicated the octahedral site as the most stable one for the carbon interstitial and the tetrahedral site as the saddle point for carbon jump from one octahedral site to another (Tapasa *et al.*, 2007). It was shown that the iron lattice volume expands owing to a C atom addition to self-interstitial atom clusters. At 300 K a cluster of seven self-interstitial atoms with one or two C atoms was found to be essentially immobilized. The cluster co-migrated with C atoms at 600 and 900 K. Dissociation of carbon from the iron cluster at 1200 K was reported.

The self-diffusion coefficients of carbon at 773 K were determined in both cementite and Hägg carbide under high carburizing atmospheres (Schneider & Inden, 2007). Metal dusting was applied to limit graphite deposition. The mechanism of carbon diffusion is not known and the carbon self-diffusion coefficient is dependent on the chemical potential difference between the surfaces and interfaces of phases containing different stoichiometric abundances of carbon.

The accurate structure determination of the carbides during FTS conditions is challenging, and further complicated by the small crystallite size of the powders (Herranz *et al.*, 2006; Niemantsverdriet *et al.*, 1980; du Plessis *et al.*, 2007; Hägg, 1931; Retief, 1999; Senateur, 1962). The meta-stable carbides are very sensitive to exposure to air/water and changes in temperature, which may result in rapid deactivation of the working catalyst owing to oxidation of χ-HC to iron oxide, a step-wise decarburization to cementite (θ-Fe_3C), carbon formation and/or sintering. However, the fundamental understanding of the catalysis process and the focused development towards more efficient catalyst using molecular dynamics tools requires a better understanding of the precise interaction between carbon and iron, and the precise carbide structure and distribution during FTS.

Recently, the crystal structure was re-determined by laboratory powder X-ray diffraction and selected-area electron diffraction (du Plessis *et al.*, 2007). The agreement of structure factors between the calculated and experimental powder patterns was significantly improved when using the triclinic structure instead of the monoclinic structure as previously reported by Senateur (1962) of χ-HC. Small but statistically significant differences (Steynberg *et al.*, 2008) in the refinement parameters when using monoclinic and pseudo-monoclinic structures of χ-HC exposed the need for higher-resolution synchrotron X-ray diffraction data. The pseudo-monoclinic crystal structure was re-determined from selected-area electron diffraction and powder X-ray diffraction by using simulated annealing, a direct-space structure determination algorithm in *Topas* (Coelho, 2000). It had to be determined whether the bulk structure of χ-HC extended to the surface of the particles, since this will be the interface available for FTS. Quantitative phase analysis using total-scattering analysis (PDF) was used to determine whether amorphous surface species exist on the χ-HC crystallites. In this manuscript we report on the results of the synchrotron X-ray powder diffraction experiments undertaken on beamline ID31 at the ESRF, Grenoble, France. In addition to conventional high-resolution Bragg scattering, the available range in diffraction angles (or rather Fourier space) further allowed the total-scattering analysis of the diffractogram using the PDF approach (Qiu *et al.*, 2004).

2. Experimental

A synthetic powder sample with particle sizes between 5 and 40 µm (Fig. 1) containing mainly χ-HC was prepared by carburization of iron with carbon monoxide at 603 K for 6 h. The individual grains are of the order of tens of nanometres (as determined by Rietveld refinement) and are not visible in Fig. 1.

The sample contained no catalysis promoters and can be considered to be a model Fischer–Tropsch catalyst. χ-HC was passivated at room temperature by exposing the sample to 0.5% oxygen in helium for 2 h to prevent oxidation during unloading of the iron carbide. The unloaded powder was packed in a 0.50 mm capillary. The diffraction experiment was undertaken on beamline ID31 at the ESRF. The wavelength was set to 0.3947 Å, equivalent to 31.4 keV. The diffractogram was collected to a maximum angle of 45° 2θ (0.0085° 2θ step size) to obtain the resolution required for accurate structure

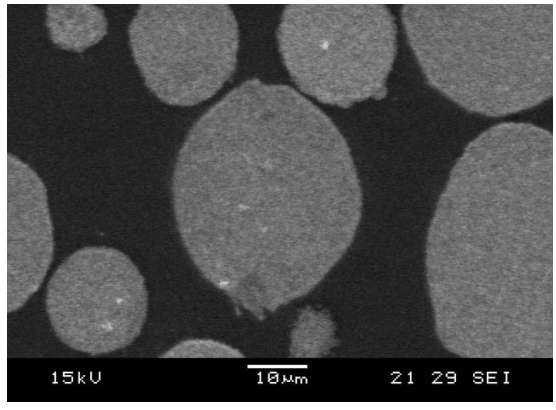

Figure 1
SEM back-scattered image of a Hägg carbide sample.

determination and refinement, as well as the PDF analysis. Longer counting times were used at higher Q-space values. The Q-space probed was thus 1.11 to 12.18 Å^{-1}. A reference standard, LaB_6, was measured for characterizing the experimental configuration. The software package *Topas 4* was used for Rietveld refinement. The PDF was determined by direct Fourier transform of the total X-ray scattering data using the software *PDFGetX2* (Qiu *et al.*, 2004).

3. Results

3.1. Results from Rietveld analysis

The basic crystal structure of χ-Hägg was re-determined by laboratory powder X-ray diffraction and selected area electron diffraction (du Plessis *et al.*, 2007), and the current measurements on ID31 follow essentially the same approach and are therefore reported here in slightly abbreviated fashion. The fundamental parameter approach was used to deconvolute instrumental and sample broadening observed in the diffractogram. The instrumental broadening was determined by refinement of a reference LaB_6 diffractogram, using instrumental broadening parameters as available in *Topas 4*. The instrumental broadening parameters were then fixed during Rietveld refinement of the χ-HC diffractogram. Line broadening observed for the individual crystalline phases was then modelled using the appropriate phase-dependent parameters available in *Topas 4*. During Rietveld refinement of the final χ-Hägg carbide structure using the pseudo-monoclinic space group $P\bar{1}$ the atomic displacement parameters of all the Fe atoms in the phases were restrained as a common isotropic parameter which refined to a value of u = 0.25 (2) Å^2 and the common isotropic parameter for the C atoms in the iron carbide phases refined to u = 0.01 (3) Å^2. The isotropic atomic displacement parameter of the C atoms in χ-Hägg carbide was restrained with a minimum limit of 0.01 Å^2, as this parameter diverged to negative values during an unconstrained Rietveld refinement. All atomic sites in the crystalline phases were fully occupied (site occupancy factor = 1). The published structures of χ-HC (du Plessis *et al.*, 2007), θ-Fe_3C (Meinhardt & Krisement, 1962) and α-Fe (Swanson *et al.*, 1955) were used. The sample contained amorphous carbon formed during preparation of the sample and this was modelled as a single broad peak and therefore excluded from the quantitative phase analysis. The crystalline size broadening contribution to the χ-HC reflections was modelled with a Lorentzian function and the volume weighted mean column height L_{Vol} (Snyder *et al.*, 1999) was found to be 36 (1) nm from the Rietveld refinement. Similarly, the strain broadening contribution was modelled using a Voigt function and the apparent strain broadening value was found to be ε_0 = 0.075 (2). The Rietveld refinement approach was as follows. The instrumental broadening contribution was determined from a refinement of the LaB_6 standard. This instrument parameter file was then used for the Rietveld refinement of the χ-HC sample. After determination of the zero error [0.004 (1) Å], this value was fixed and the lattice parameters and relative atomic coordinates of χ-HC were refined. The lattice parameters and relative atomic coordinates of θ-Fe_3C and α-Fe were fixed to the published values for the initial Rietveld refinement. Upon obtaining an improved fit of χ-HC to the experimental diffractogram, the θ-Fe_3C and α-Fe lattice parameters and average crystallite sizes were refined. The improved values were then fixed and the final step was to refine the lattice parameter, relative atomic coordinates and average crystallite size of χ-HC. The agreement values (Young, 1995) were R_{wp} = 9.25%, S = 2.9% and R_{Bragg} = 4.0%, as compared with R_{wp} = 12.7%, S = 4.0% and R_{Bragg} = 6.6% when refining the same synchrotron diffraction data using the structure as published by Retief (1999). The experimental and theoretical diffractograms of χ-HC can be seen in Fig. 2, together with a visualization of the unit cell.

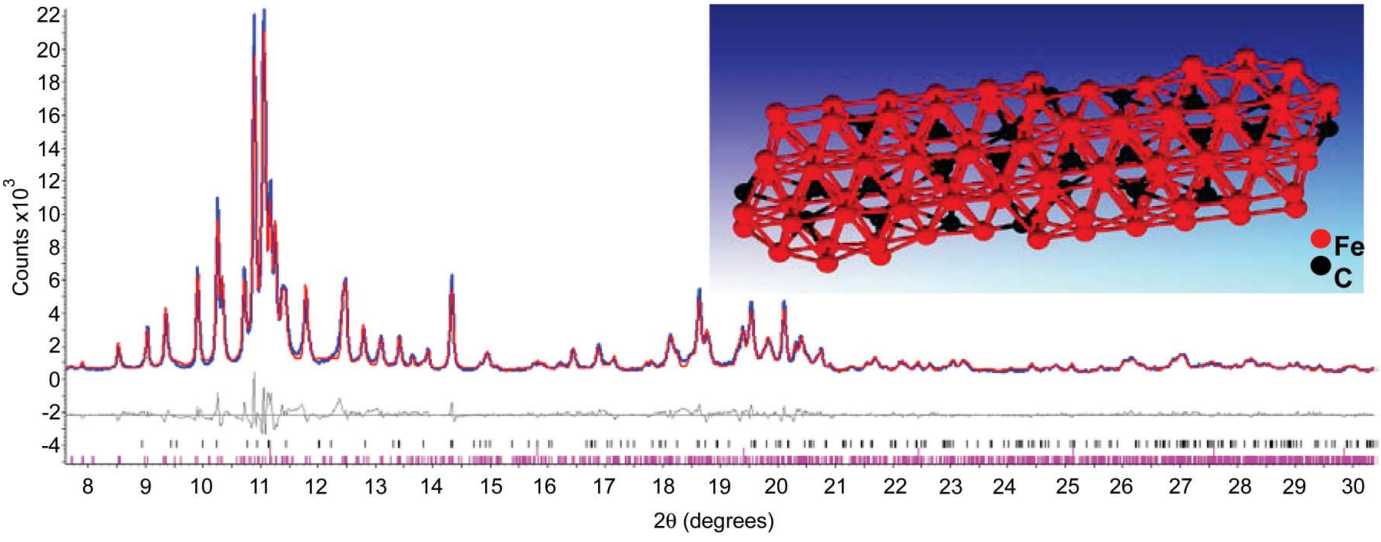

Figure 2
Experimental (blue) and theoretical (red) diffractograms of χ-HC, θ-Fe_3C and α-Fe (° 2θ, λ = 0.39466 Å). The inset shows the refined crystal structure (see also Fig. 5).

3.2. Results from PDF analysis

Unlike most conventional X-ray diffraction data, the diffractograms collected on ID31 lend themselves to analysis *via* a PDF approach. The PDFs [$G(r)$] for χ-HC, θ-Fe_3C and α-Fe were calculated and refined using *PDFGui* software (Farrow *et al.*, 2007). The fit between the experimental and theoretical PDFs is shown in Fig. 3. The lattice parameters, relative abundances of the phases and relative atomic coordinates and atomic displacement parameters thereof were refined for both the monoclinic and pseudo-monoclinic structures of χ-HC. Since the bulk crystalline phases were identified and quantified during the Rietveld refinement analysis, these phases were used as starting models for the PDF analysis. The relative abundances and atomic coordinates of all the phases (χ-HC, θ-Fe_3C, α-Fe) were refined as well as the isotropic atomic displacement parameters. A spherical nanoparticle shape was assumed and found to be sufficient. The peaks visible on the experimental PDF do not have an increased broadening at higher R values, indicating that there is no stacking disorder visible up to 20 Å. The PDF does not display a typical nanocrystalline decrease of peak intensities and this result correlates with the large average crystallite size obtained from Rietveld refinement, *i.e.* 36 (1) nm. An R_{wp} value of 12.9% and reduced χ^2 value of 15.4% was obtained when fitting the experimental and theoretical PDFs when using the pseudo-monoclinic crystal structure of χ-HC, indicating that the bulk phases extended to the surface of the particles. The interatomic distances in the range 1.8–2.2 Å are assigned to iron to carbon, mainly from χ-HC, and the peak intensity and width match well, indicating that all interatomic distances of 1.8–2.2 Å in the sample are explained by the phases included in the PDF refinement. The larger interatomic distances can be assigned to iron–iron, iron–carbon and carbon–carbon interactions.

The presence of 1–2 wt% α-iron (reactant) was detected in the synchrotron X-ray diffractogram when carrying out the Rietveld refinement, which was not visible using laboratory X-ray data, probably owing to the small crystallite size (44 nm, from Rietveld refinement) and peak overlap of the (011) reflection of α-iron with the χ-HC (121) reflection. The α-iron phase was included during a trial Rietveld refinement of the laboratory X-ray data, but refined to zero. The (011) reflection of α-iron in the synchrotron X-ray diffractogram is indicated by a red arrow in Fig. 4.

However, using the PDF approach (Farrow *et al.*, 2007; Qiu *et al.*, 2004) it was possible to refine the nanocrystalline structure of χ-HC, which confirmed the triclinic structure to be prevalent in the synthetically prepared χ-HC. The lattice parameters, relative abundances, atomic displacement parameters and relative atomic coordinates of χ-HC were optimized during the PDF refinements. A comparison of the relative abundances of the crystalline phases obtained from the Rietveld refinements (using the $C2/c$ and $P\bar{1}$ crystal structures of χ-HC) and the agreement values are listed in Table 1; it is clear from the table that the crystal structure of χ-HC is indeed $P\bar{1}$, as indicated by improved agreement values.

Table 1
Relative abundances of phases.

	Rietveld $C2/c$	Rietveld $P\bar{1}$	PDF $C2/c$	PDF $P\bar{1}$	Mössbauer spectroscopy
Relative abundances (wt%)†					
χ-HC	80 (1)	84 (1)	93 (1)	90 (3)	85 (1)
θ-Fe_3C	17 (1)	15 (1)	5 (1)	8 (3)	15 (1)
α-Fe	2 (0.3)	1 (0.1)	2 (0.2)	2 (1)	–
R_{wp} (%)	12.74	9.01	15.5	12.9	
R_{Bragg} (χ-HC) (%)	6.59	4.0		–	
S (%)	4.0	2.9	21.5	15.4	

† Results normalized to iron and iron carbides.

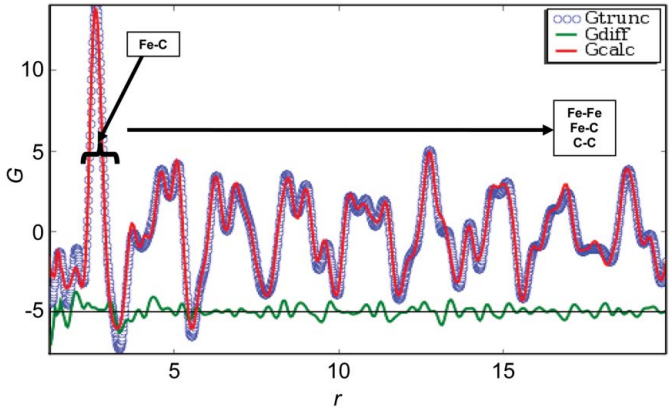

Figure 3
The PDF $G(r)$ for χ-HC, θ-Fe_3C and α-Fe (blue) with the refined fit of the model (red) and the difference pattern (green).

4. Discussion

Theoretically, the optimal packing of Fe atoms around the central C atoms in the monoclinic structure is simple trigonal

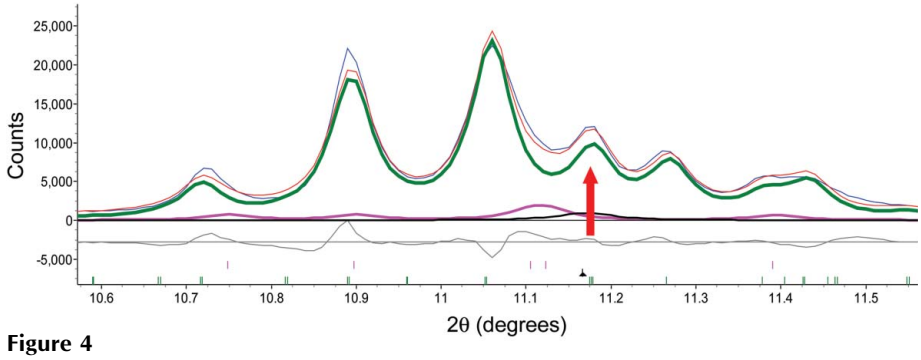

Figure 4
Experimental (blue) and theoretical (red) diffractograms and contributions of χ-HC (green), θ-Fe_3C (pink) and α-Fe (black) (° 2θ, λ = 0.39466 Å).

Table 2
Relative atomic coordinates of χ-HC, and deviations from the theoretical *C*2/*c* optimal packing.

Atom	x	Δx	y	Δy	z	Δz
Fe1a	0.3532 (1)	−0.007	0.3269 (1)	0.005	0.4281 (1)	−0.009
Fe1b	0.6512 (1)	0.002	0.8179 (2)	0.014	0.0856 (3)	−0.005
Fe1c	0.1539 (1)	0.000	0.3353 (3)	−0.003	0.0898 (3)	−0.009
Fe1d	0.8370 (1)	0.010	0.8447 (2)	−0.013	0.4179 (2)	0.002
Fe2a	0.4558 (1)	0.008	0.8387 (3)	−0.003	0.2939 (3)	0.012
Fe2b	0.5275 (1)	0.009	0.3505 (3)	−0.015	0.1979 (3)	−0.004
Fe2c	0.0378 (1)	−0.002	0.8288 (3)	0.007	0.1820 (2)	0.012
Fe2d	0.9677 (1)	−0.004	0.3358 (3)	0.000	0.3087 (3)	−0.003
Fe3a	0.2523 (1)	−0.002	0.8270 (3)	0.000	0.2488 (3)	0.001
Fe3b	0.7462 (1)	0.004	0.3291 (3)	−0.003	0.2489 (3)	0.001
C1	0.3641 (5)	0.006	0.552 (1)	−0.016	0.074 (1)	0.019
C2	0.6109 (5)	0.019	0.010 (1)	0.026	0.358 (1)	0.049
C3	0.1357 (2)	−0.006	0.545 (1)	−0.009	0.434 (1)	−0.027
C4	0.887 (1)	−0.017	0.107 (1)	−0.071	0.067 (1)	0.026

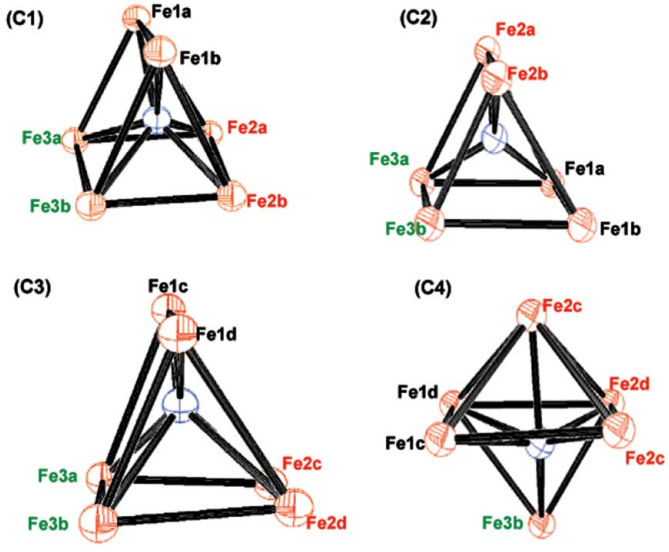

Figure 5
The three different types of distorted trigonal prisms and an octahedron of iron (shaded) around the central C atoms (no shading) for all four C atoms in the unit cell.

prisms (Hirotsu & Nagakura, 1972; Dirand & Afqir, 1983). In the $P\bar{1}$ space group both the Fe and C atoms are allowed additional positional freedom during the refinement. This provided a better fit of the experimental diffractogram and suggests that the Fe atoms in the unit cell are arranged in three different types of distorted trigonal prisms and an octahedron around the central C atoms (compare Fig. 5).

The PDF approach was used to refine the nanocrystalline structure of χ-HC. From the agreement between the Rietveld and PDF refinements it can be deduced that the bulk structure probably extends to the surface of the powder particles. Differences in relative abundances between Rietveld and PDF quantitative refinements usually indicate local structural disorder (Egami & Billinge, 2003). The distortions of the trigonal prisms are thus not due to local disorder but are possibly due to the mobility of carbon in the bulk structure.

The relative atomic coordinates as fractions of the unit cell of χ-HC are listed in Table 2. The values Δx, Δy and Δz indicate the deviations in the relative atomic coordinates of the atoms from those in the monoclinic structure (*C*2/*c*). These relative atomic coordinate displacement values suggest that the C atoms could be mobile in the χ-HC crystal structure.

To summarize, high-resolution synchrotron X-ray diffraction data were obtained on beamline ID31 at the ESRF and confirmed the pseudo-monoclinic structure of χ-HC. In addition to confirmation of the true crystal structure of χ-HC, the presence of 1–2 wt% iron was detected in the sample using synchrotron X-rays, which was not visible using laboratory X-ray diffraction. Using the PDF approach it was also possible to refine the nanocrystalline structure of χ-HC, which proved the triclinic structure to be prevalent in the unloaded catalysts. It is also clear from comparing Rietveld and PDF quantitative phase analyses that the bulk χ-HC structure extends to the surface of the χ-HC particles. The Fe atoms are located in three distorted prismatic trigonal and one octahedral arrangement around the central C atoms, an arrangement which is significantly different from the monoclinic structure of χ-HC as described and reported previously.

We gratefully acknowledge Sasol Technology R&D Pty Ltd, South Africa, for funding, and acknowledge the ESRF (Grenoble, France) for provision of beam time on the high-resolution powder diffraction beamline ID31.

References

Campos, A., Lohitarn, N., Roy, A., Lotero, E., Goodwin, J. G. Jr & Spivey, J. J. (2010). *Appl. Catal. A*, **375**, 12–16.
Coelho, A. A. (2000). *J. Appl. Cryst.* **33**, 899–908.
Dirand, M. & Afqir, L. (1983). *Acta Metall.* **31**, 1089–1107.
Dry, M. E. (1990). *Catal. Lett.* **7**, 241–252.
Egami, T. & Billinge, S. J. L. (2003). *Underneath the Bragg Peaks: Structural Analysis of Complex Materials.* Oxford: Pergamon/Elsevier.
Faraoun, H. I., Zhang, Y. D., Esling, C. & Aourag, H. (2006). *J. Appl. Phys.* **99**, 093508.
Farrow, C. L., Juhas, P., Liu, J. W., Bryndin, D., Bozin, E. S., Bloch, J., Proffen, T. & Billinge, S. J. L. (2007). *J. Phys. Condens. Matter*, **19**, 335219.
Hägg, G. (1931). *Phys. Chem.* B**12**, 33–56.
Herranz, T., Rojas, S., Perez-Alonso, F. J., Ojeda, M., Terreros, P. & Fierro, J. L. G. (2006). *J. Catal.* **243**, 199–211.
Hirotsu, Y. & Nagakura, S. (1972). *Acta Metall.* **20**, 645–655.
Königer, A., Hammerl, C., Zeitler, M. & Rauschenbach, B. (1997). *Phys. Rev. B*, **55**, 8143–8147.
Mansker, L. D. (1999). PhD thesis, The University of New Mexico, NM, USA.
Meinhardt, D. & Krisement, O. (1962). *Arch. Eisenhuettenwes.* **33**, 493–499.
Niemantsverdriet, J. W., Van der Kraan, A. M., Van Dijk, W. L. & Van der Baan, H. S. (1980). *J. Phys. Chem.* **84**, 3363–3370.
Pérez-Alonso, F. J., Herranz, T., Rojas, S., Ojeda, M., López Granados, M., Terreros, P., Fierro, J. L. G., Gracia, M. & Gancedo, J. R. (2007). *Green Chem.* **9**, 663–670.
Plessis, H. E. du, de Villiers, J. P. R. & Kruger, G. J. (2007). *Z. Kristallogr.* **222**, 211–217.
Qiu, X., Thompson, J. W. & Billinge, S. J. L. (2004). *J. Appl. Cryst.* **37**, 678.

Retief, J. J. (1999). *Powder Diffr.* **14**, 130–132.
Riedel, T. & Schulz, H. (2003*a*). *Topics Catal.* **26**, 1–4.
Riedel, T. & Schulz, H. (2003*b*). *Topics Catal.* **26**, 41–54.
Sarkar, A., Seth, D., Dozier, A. K., Neathery, J. K., Hamdeh, H. H. & Davis, B. H. (2007). *Catal. Lett.* **117**, 1–17.
Schneider, A. & Inden, G. (2007). *CALPHAD*, **31**, 141–147.
Senateur, J. P. (1962). *C. R. Acad. Sci.* **255**, 1615–1616.
Snyder, R. L., Bunge, H. J. & Fiala, J. (1999). Editors. *Microstructure Analysis from Diffraction*, pp. 94–124. Oxford University Press.
Steynberg, P. J., van den Berg, J. A. & Janse van Rensburg, W. (2008). *J. Phys. Condens. Matter*, **20**, 064238.
Swanson, H. E., Fuyat, R. K. & Ugrinic, G. M. (1955). *Standard X-ray Diffraction Powder Patterns*, *National Bureau of Standards Circular* 539, IV, p. 75. Washington, DC: National Bureau of Standards.
Tapasa, K., Barashev, A. V., Bacon, D. J. & Osetsky, Y. N. (2007). *J. Nucl. Mater.* **361**, 52–61.
Young, R. A. (1995). Editor. *The Rietveld Method.* Oxford University Press.